Preclinical zebrafish model for organophosphorus intoxication: neuronal hyperexcitation, behavioral abnormalities and subsequent brain damages

Alexandre Brenet[1], Julie Somkhit[1], Rahma Hassan-Abdi[1], Constantin Yanicostas[1], Alexandre Igert[2], Dominique Saurat[3], Nicolas Taudon[3], Roxane Loyant[4], Mathieu Porceddu[4], Gregory Dal-Bo[2], Florian Nachon[2], Nina Dupuis[2#], and Nadia Soussi-Yanicostas[1#]*

[1] Université de Paris, NeuroDiderot, Inserm, F-75019 Paris, France

[2] Institut de Recherche Biomédicale des Armées (IRBA), Département de toxicologie et risques chimiques, F-91 220 Brétigny-sur-Orge, France.

[3] Institut de Recherche Biomédicale des Armées (IRBA), Unité de développements analytiques et bioanalyse, F-91 220 Brétigny-sur-Orge, France.

[4] Mitologics SAS, Faculté de Médecine, 94000 Créteil, France

# These authors contributed equally to this work.

* Corresponding authors:

Dr Nadia Soussi-Yanicostas
Neurodiderot
INSERM U1141
48 boulevard Serurier
75019 Paris
France
e-mail : nadia.soussi@inserm.fr
phone : +33 (0)1 40 03 19 31

ABSTRACT

As key compounds for modern cultivation practices, organophosphorus (OP)-containing pesticides have become an important public health and environmental issues, worldwide, causing millions human intoxications each year. OP poisoning induces cholinergic syndrome, associating irreversible brain damages with epileptic seizures, possibly ending in life-threatening status epilepticus. Existing countermeasures are life-saving, but insufficiently effective to prevent long lasting neuronal consequences, emphasizing the dire need for animal models mimicking OP poisoning as tools to identify novel anti-OP countermeasures. Here, we used diisopropylfluorophosphate (DFP), a prototypic and moderately toxic OP compound, to generate a zebrafish OP intoxication model and study the consequences of DFP exposure on neuronal activity, larvae behaviour and neuron network organization. DFP poisoning caused marked acetylcholinesterase (AChE) inhibition, resulting in paralysis, decreased oxygen consumption, overexpression of c-Fos neuron activity marker, increased neuron apoptosis and epileptiform seizure-like activity, which was partially alleviated by diazepam treatment. DFP-exposed larvae also showed altered neuron networks with increased accumulation of NR2B-NMDA receptor combined with decreased GAD65/67 and gephyrin protein accumulation. Thus, we described a zebrafish model of DFP poisoning, which should (i) provide important insights into the pathophysiological mechanisms underlying OP intoxication and ensuing brain damage, and (ii) help identify novel therapeutic agents to restore CNS functions following acute OP poisoning.

KEYWORDS: Zebrafish model; Organophosphorus (OP) intoxication; Epileptiform seizure; Neuron toxicity, Diisopropylfluorophosphate (DFP); Respiratory failure.

46 **1. INTRODUCTION**

47 Organophosphorus (OP) compounds are highly toxic molecules used as lethal weapons in
48 both war situations and terrorist attacks, but also as key chemical pesticides to combat pests and
49 parasites. As the result of their massive use for agricultural purposes worldwide, OP poisoning
50 represents today a major public health issue with 3 million severe intoxications reported annually
51 and more than 200,000 deaths, primarily suicides[1–4]. OP are potent inhibitors of cholinesterase,
52 including acetylcholinesterase (AChE), causing massive acetylcholine accumulation at cholinergic
53 synapses and overstimulation of cholinergic receptors at both neuromuscular junctions and CNS
54 cholinergic synapses[5]. OP-induced cholinergic hyperactivity in the brain can provoke epileptic
55 seizures, which, if not rapidly treated, may turn into life-threatening status epilepticus[6]. Besides
56 immediate toxicity, survivors of OP poisoning also face long-term comorbidities that include
57 psychomotor defects, cognitive deficits and recurrent seizures[7,8]. Existing countermeasures against
58 OP poisoning are life-saving but not yet sufficiently effective against seizure occurrence and brain
59 damage. There is thus an urgent need for new therapeutic agents.

60 The generation and characterization of an animal model of OP intoxication faithfully
61 mimicking the consequences of OP poisoning in humans is urgently needed both for a better
62 understanding of OP poisoning pathophysiology and for high-throughput screening of therapeutic
63 entities counteracting the toxicity of these compounds. Rodent OP intoxication models are not fully
64 pure, because respiratory blockade induced by OP requires mandatory co-administration of both
65 cholinergic agonist and AChE reactivator with the tested OP compounds. As an alternative
66 vertebrate species, we describe here a preclinical zebrafish model of OP poisoning and characterize
67 the neuron defects induced.

68 Over the past decade, besides its skyrocketing use as a human disease model [9–13], the zebrafish has
69 become one of the leading animal models for toxicology research[14]. This small and easy-to-breed
70 fish offers significant advantages for in vivo drug discovery and neurotoxicology investigations,
71 including a CNS that displays an overall organization similar to that of mammals and full
72 conservation of different neuron types, neurotransmitters and glial cell types[15–19].

73 To model OP intoxication in zebrafish, we used diisopropylfluorophosphate (DFP), an
74 analogue of the chemical warfare agents sarin and soman, which promotes potent AChE inhibition.
75 However, DFP is safer, less volatile, and much less dangerous for experimentation purposes than
76 soman, making it an OP fully suited to experimental research. It has been shown that acute DFP
77 intoxication in rats induces seizures[20] and causes neurodegeneration, memory impairment and
78 neuroinflammation[20,21]. DFP has been used to model seizures with subsequent behavioral deficits
79 in rodents[22–25]. However, while it has long been known that acute intoxication with OP nerve agents,
80 such as sarin, soman and DFP, causes neuropathological changes in the brain in both human
81 patients and animal models[8,21,26,27], this brain damage and its extent remain poorly understood.

82 By combining behavioral analysis, respiration measurements, in vivo brain calcium
83 imaging and molecular and immunocytochemical approaches, we showed that larvae exposed to
84 DFP displayed motor paralysis correlated with inhibition of AChE activity and depressed
85 respiration. DFP-treated larvae also showed increases in both c-Fos expression and neuronal
86 calcium uptakes, which reflect epileptiform seizures. We also observed a marked increase in neuron
87 apoptosis and excitatory NR2B-NMDA receptor sub-unit accumulation, combined with a
88 decreased accumulation of both GAD65/67 and gephyrin proteins, reflecting a shift of the synaptic
89 balance toward excitatory states.

90 **2. MATERIALS AND METHODS**

91 **2.1 Fish husbandry and zebrafish lines**

92 Zebrafish were kept at 26–28 °C in a 14 h light/10 h dark cycle. Embryos were collected by
93 natural spawning and raised in E3 solution at 28.5 °C. To inhibit pigmentation, 0.003% 1-phenyl-
94 2-thiourea was added at 1 day post-fertilization (dpf). Tg[HuC:GCaMP5G] transgenic line was
95 used to monitor calcium activity, otherwise wild-type AB embryos were used. All the animal
96 experiments were conducted at the French National Institute of Health and Medical Research
97 (INSERM) UMR 1141 in Paris in accordance with European Union guidelines for the handling of
98 laboratory animals (http://ec.europa.eu/environment/chemicals/lab_animals/home_en.htm), and
99 were approved by the Direction Départementale de la Protection des Populations de Paris and the
100 French Animal Ethics Committee under reference No. 2012-15/676-0069.

101 **2.2 DFP treatment**

102 Diisopropylfluorophosphate (DFP) was purchased from Sigma Aldrich. A stock solution
103 (5.46 mM), stored at -20°C, was diluted extemporaneously to 15 μM in 1% DMSO. Control
104 zebrafish larvae were treated with 1% DMSO.

105 **2.3 DFP stability**

106 Ranging amounts of DFP were diluted in 1% DMSO, and 200 μL water samples were
107 removed at different incubation times (0, 2, 4, 6 and 24 h; n = 3 per condition) and were stored at
108 -20 °C until extraction. 360 μL of ethyl acetate (VWR) was added to 180 μL of the sample. After
109 vigorous shaking, an aliquot (100 μL) of organic phase was extracted (recovery > 90%) and stored

110 at 4 °C until analysis by gas chromatography-mass spectrometry (GC-MS). GC-MS analyses were
111 conducted with a gas chromatograph (Agilent 6890N) coupled to a quadrupole mass spectrometer
112 equipped with an EI source (Agilent MSD5973). After a pulsed splitless injection (40 psi) at
113 220 °C, the GC separation was performed on an Rtx-OPP2 column (Restek, 30 m x 0.25 mm x
114 0.25 μm) using a linear ramp from 40 °C to 280 °C (20 °C/min). The mobile phase was helium
115 (99.9995%) at a flow rate of 1.2 mL/min. The source and quadrupole temperatures were set at
116 230 °C and 150 °C. Acquisition was performed in the SIM (single ion monitoring) mode (m/z 101
117 and 127 as quantifier and qualifier ions). Operating software was MassHunter Workstation
118 Quantitative analysis version B.09.00/Build 9.0.647.0. DFP concentrations were calculated based
119 on a linear calibration curve (individual residuals within ±20%), obtained with solutions of DFP in
120 ethyl acetate between 0.05 and 1.35 μg/mL.

121 **2.4 Acetylcholinesterase activity**

122 Five dpf zebrafish larvae (20 larvae per sample) were collected at 2 h, 4 h, 6 h post-exposure
123 to DFP and stored at −80 °C for further analysis. Samples were homogenized in 50 mM phosphate
124 buffer (pH 7.4)/0.5% Tween using Precellys® homogenizer with 1.4 mm ceramic beads and
125 centrifuged at 10,000 × g (4 °C) for 10 min. The resulting supernatants were collected and stored
126 at −80 °C. Total protein concentrations were determined using the DC Protein Assay (Bio-Rad)
127 and all the samples were diluted to 1.2 mg/mL. AChE activity was determined by adding 1 mM
128 acetylthiocholine (Sigma) and 0.22 mM 5,5′-dithiobis-2-nitrobenzoic acid (DTNB, Sigma) to the
129 sample (0.03 mg/mL of total proteins), the formation of the product resulting from the reaction
130 between thiocholine and DTNB at 25 °C was monitored for 30 min at 412 nm with a microplate

131 reader. All the samples were assayed in duplicate. The final results were expressed as percentages
132 of average control activity.

133 **2.5 Measurement of oxygen consumption**

134 Five dpf larvae were exposed to DFP or vehicle (1% DMSO) for 4.5 h and then transferred
135 to 96-well microplates (Greiner Bio-One International) (7 individuals per well) containing 90 μL
136 of E3 medium and 10 μL of 35 μg/mL MitoXpress Xtra (MitoXpress Xtra Reagent Pack, Agilent
137 Technologies) that enables real-time measurement of extracellular oxygen consumption in living
138 larvae. A volume of 100 μL of mineral oil (MitoXpress Xtra Reagent Pack, Agilent Technologies)
139 was added to seal the wells and isolate the reaction medium from ambient air oxygen. Oxygen
140 consumption was then measured in real time for 90 min at 28 °C in a 96-well plate using a
141 spectrofluorimeter (Tecan Spark: $\lambda_{excitation}$ 380 nm, $\lambda_{emission}$ 650 nm). The areas under the linear
142 portion of the curve were used to determine O_2 consumption rates.

143 **2.6 Hematoxylin/eosin staining**

144 Five dpf larvae were exposed to DFP or vehicle (1% DMSO) and then anesthetized using
145 0.01% tricaine, fixed with 10% formaldehyde, paraffin-embedded and sectioned. Sections were
146 deparaffinized and rehydrated before hematoxylin and eosin staining. Freshly stained sections were
147 treated with ethanol and xylene, and then mounted in Pertex medium. Sections were imaged using
148 a Nikon Eclipse microscope (E-200) equipped with a digital sight (Nikon).

149 **2.7 Zebrafish larval locomotor activity**

150 Locomotor activity of 5 dpf zebrafish larvae was performed as previously described in
151 Brenet et al, 2019[11].

152 **2.8 RT-qPCR**

153 For RNA isolation, larvae were homogenized using a syringe equipped with a 26G needle
154 (seven larvae per sample) using the RNA XS Plus kit (Qiagen, Hilden, Germany). cDNA was
155 synthesized using the iScriptTM cDNA Synthesis Kit (Bio-Rad, Munich, Germany) and qPCR was
156 performed using iQTM SYBR Green Supermix (Bio-Rad). Samples were run in triplicate.
157 Expression levels were normalized to that of eef1a1. The primers (Eurofins Genomics, Ebersberg,
158 Germany) used were: c-fos-forw, 5'-AAC CAG ACT CAG GAG TTC AC-3'; c-fos-rev, 5'-GGA
159 GAA AGC TGT TCA GAT CTG-3'; ee1fa1-forw, 5'-CCA CTA CGA CTG GTC ACC TC-3';
160 and ee1fa1-rev, 5'-AAG CTT GTC CAG AAC CCA GG-3'.

161 **2.9 Neuronal calcium uptake imaging**

162 Calcium imaging of 5 dpf zebrafish larvae was performed as previously described in Brenet
163 et al, 2019[11].

164 **2.10 Diazepam treatment**

165 Five dpf Tg[Huc:GCaMP5G] larvae were exposed to 15 μM DFP for 5 h and then
166 pancuronium-paralyzed and embedded in 1.1% low-melting agarose in the center of a 35 mm glass-
167 bottomed dish covered with E3 solution containing 300 μM pancuronium bromide. Calcium
168 uptakes were recorded for 30 min prior to diazepam (40 μM DZP, Sigma) addition and calcium

169 activity was then monitored for an additional hour. Calcium activity was measured as described in
170 Brenet et al, 2019[11].

171 **2.11 Apoptosis labeling**

172 Neuronal cell death was visualized and quantified as previously described in Brenet et al,
173 2019[11].

174 **2.12 Immunohistochemistry**

175 For synapse protein immunostaining, zebrafish larvae were fixed using 4% formaldehyde,
176 then directly immersed in 10% sucrose at 4 °C and incubated overnight, embedded in 7.5%
177 gelatin/10% sucrose solution, flash frozen in isopentane at -45 °C and stored at -80 °C until use.
178 When needed, frozen embedded zebrafish larvae were cut into 20 μm cryostat sections, which were
179 mounted on superfrost slides. Sections were then washed, blocked and permeabilized with 0.2%
180 gelatin/0.25% Triton X-100 diluted in PBS. Sections were incubated overnight at room temperature
181 with either anti-gephyrin antibodies (1:100, rabbit polyclonal, Abcam, Ab185993), anti-NR2B-
182 NMDA antibodies (1:200, rabbit polyclonal, Abcam, Ab35677), or anti-GAD65/67 antibodies
183 (1:500, rabbit polyclonal, Abcam, Ab11070). Sections were then washed three times in PBS (5 min
184 each time) and incubated for 2 h at room temperature, in the dark, with an anti-rabbit IgG
185 conjugated with Alexa 488 fluorophore (1:500, mouse, Molecular Probes, A-21206). Sections were
186 finally counterstained for 10 min with 0.3% DAPI, and after a final wash, sections were mounted
187 in Fluoromount medium and stored at 4 °C.

188 **2.13 Synapse quantification**

189 Sections hybridized with anti-gephyrin antibodies were imaged at full resolution (voxel
190 size: 0.063 x 0.063 x 0.4 μm) using an inversed Leica TCS SP8 confocal scanning system (Leica
191 Microsystems) equipped with an oil-immersion objective (Leica 40x HCPL APO CS2, numerical
192 aperture 1.30). Images were then processed with AutoQuant 3X software (Media Cybernetics) and
193 the density of post-synaptic puncta was quantified using a homemade ImageJ macro (Zsolt Csaba,
194 Inserm UMR1141). After applying a median filter on all images, a threshold was applied to
195 quantify only post-synaptic puncta. Areas of interest that comprised the optic tectum and
196 telencephalon were selected and all spots with sizes in the range 0.018–3.14 μm^2 were considered
197 as post-synaptic puncta. Post-synaptic density of gephyrin puncta was finally calculated by
198 dividing the number of puncta detected in a given region by the surface of the region. Images from
199 four independent experiments were used to calculate mean gephyrin density and corresponding
200 standard error of the mean (SEM), and to assess the statistical significance of the differences
201 observed between DFP-treated and control larvae.

202 **2.14 Quantification of GAD65/67 and NR2B accumulation**

203 Following GAD65/67 and NR2B (NR2B-NMDA) immunostaining, images of brain
204 sections were acquired using an inversed Leica TCS SP8 confocal scanning system (Leica
205 Microsystems) equipped with an oil-immersion objective (Leica 40x HCPL APO CS2, numerical
206 aperture 1.30). Images were acquired in three dimensions (48.50 x 48.50 x 20 μm) and the volume
207 occupied by stained structures was determined using MeasurementPro's Surfaces of the Imaris
208 software (Bitplane Inc., Version 9.1.2). For both GAD65/67 and NR2B/NMDA, images from three
209 independent experiments were used to calculate mean GAD65/67 and NR2B staining volumes and

210 corresponding standard errors of the mean (SEM), and to assess statistical significance of the
211 differences observed between DFP-treated and control larvae.

212 **3 RESULTS**

213 **3.1 Larvae exposed to DFP showed paralysis and acetylcholinesterase (AChE) inhibition**

214 Prior to the development of a zebrafish model of DFP poisoning, we first measured the
215 stability of this compound after dilution in fish water. Ranging amounts of DFP were diluted in
216 fish water and DFP concentrations were determined until 6 hours. Results showed that diluted DFP
217 was stable in fish water, with an average 2% loss per hour, approximately (Figure S1). Next, to
218 determine in vivo DFP toxicity in zebrafish, 5 days post-fertilization (dpf) larvae were exposed to
219 15, 20, 30, and 50 μM DFP and studied over a 24 h period. Results showed that all larvae incubated
220 in 20 μM DFP or in higher concentration, either died prior to 6 h exposure or displayed gross
221 phenotypic defects, including a curly tail and marked reductions of the head's and eyes' volumes
222 (Figure S2). As we sought to investigate DFP neurotoxicity and subsequent brain damages, we
223 selected 15 μM DFP and an exposure time of 6 h (Figure 1B), an experimental setup that did not
224 induce any visible phenotype (n = 20) when compared to control larvae exposed to 1% DMSO
225 (n = 20) (Figure 1C), nor any significant increase in larvae lethality. Histopathological analysis
226 confirmed that larvae exposed to 15 μM DFP showed no visible neurological abnormalities (Figure
227 S3).

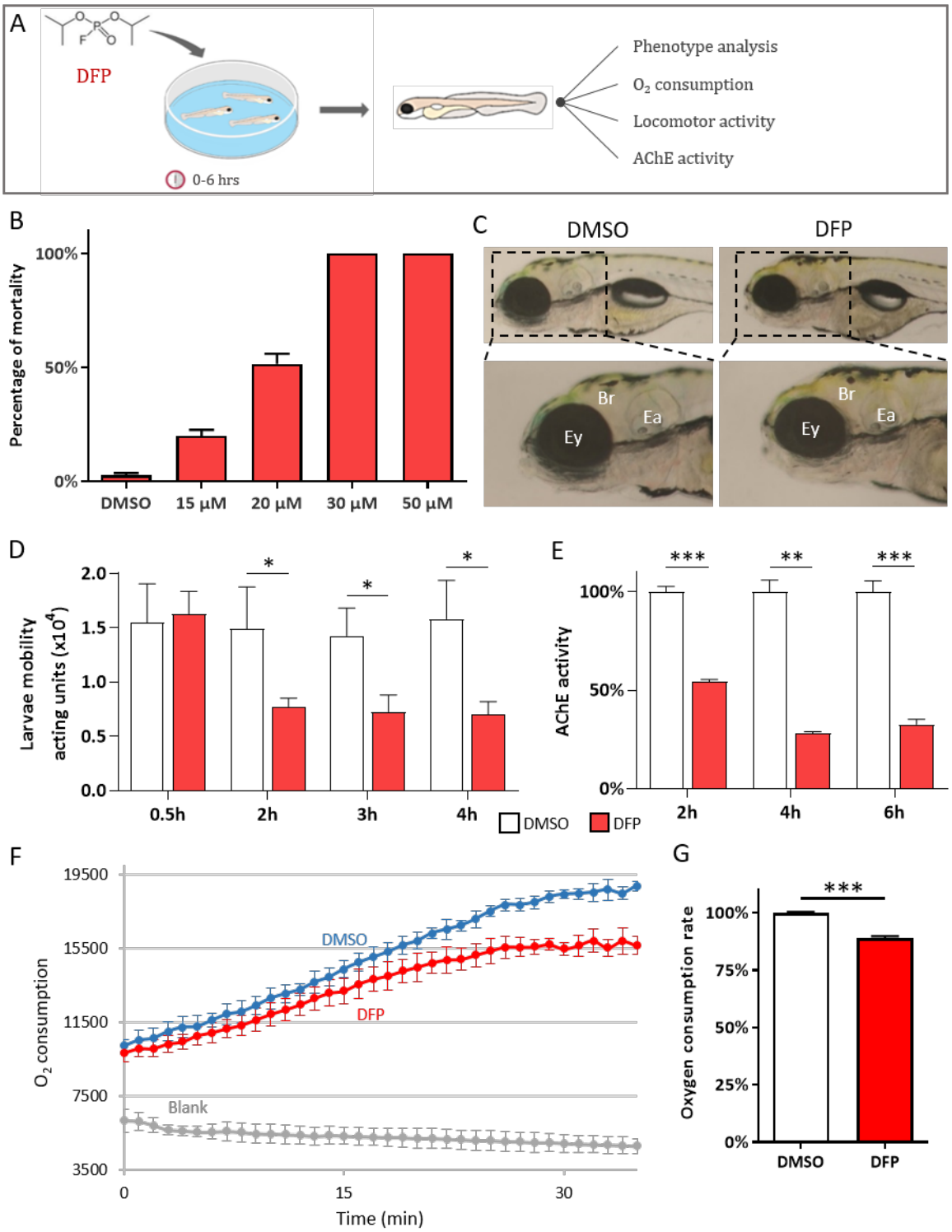

228

229 **Figure 1.** DFP-exposed zebrafish larvae displayed reduced motility, AChE inhibition and

230 respiratory failure. **A**: In the experimental set-up, 5 dpf larvae were exposed to 15, 20, 30 and 50

231 μM DFP, and larvae lethality, phenotypic defects, locomotor activity and AChE activity were
232 studied for 6 h. **B**: Lethality rates of 5 dpf larvae exposed for 6 h to 15, 20, 30 and 50 μM DFP led
233 us to select 15 μM DFP as optimal concentration (LC20). **C**: 5 dpf larvae exposed for 6 h to either
234 15 μM DFP or vehicle (DMSO), are phenotypically indistinguishable. **D**: Quantification of AChE
235 activity in larvae exposed to either 15 μM DFP (n = 5) or vehicle (DMSO) (n = 5), for 2, 4, and 6
236 h (Student unpaired t-test: **, $p < 0.01$; ***, $p < 0.001$). **E**: Locomotor activity of 5 dpf larvae
237 exposed to either 15 μM DFP (n = 48) or vehicle (DMSO) (n = 48) (Mann-Whitney test: *, $p <$
238 0.05). **F**: Real-time measurement of oxygen consumption by 5 dpf larvae exposed to either 15 μM
239 DFP or vehicle (DMSO). **G**: Quantification of oxygen consumption rate (OCR) of larvae exposed
240 to either 15 μM DFP (n = 301) or vehicle (DMSO) (n = 189) (Student unpaired t-test: ***, $p <$
241 0.001). Abbreviations: Ey, eye; Br, brain; Ea, ear.

242 **3.2 AChE inhibition, leading to paralysis and respiratory failure in DFP exposed larvae**

243 As AChE inhibition and muscle paralysis are hallmarks of OP poisoning, we measured the
244 motor activity of DFP-exposed and control larvae, by measuring the distance swum by these
245 individuals over a 30-min period. As expected, larvae exposed to DFP (n = 48) showed
246 significantly decreased motor activity compared to their control siblings (n = 48) (Figure 1D). We
247 next estimated AChE activity in larvae exposed to either 15 μM DFP (n = 5) or vehicle (DMSO
248 1%) (n = 5). We observed a 50% inhibition of AChE activity as early as 2 h after DFP exposure
249 (Figure 1E). As respiratory failure is an early consequence of OP poisoning[28,29], we next quantified
250 the respiration of larvae exposed to 15 μM DFP by calculating the extracellular oxygen
251 consumption rate (ORC) of living larvae using the MitoXpress Xtra oxygen consumption assay, a
252 simple kinetic measurement of oxygen consumption (Figure 1F). Results showed that the OCR of

253 larvae exposed to 15 μM DFP were 88.78 ± 1.00% of that observed in controls (Figure 1G, $p <$
254 0.001). Thus, after DFP exposure, zebrafish larvae displayed strong inhibition of AChE activity,
255 decreased oxygen consumption, and reduced motor activity.

256 **3.3 DFP exposure promoted neuronal hyperexcitation and apoptosis**

257 Increase in c-Fos expression, a molecular marker of activity, is observed during seizures[30],
258 and has been shown to promote epileptogenesis[31–34]. As a first attempt to evaluate the consequences
259 of DFP poisoning on neuronal activity, we studied c-Fos expression in DFP-treated and control
260 sibling larvae. Interestingly, qRT-PCR revealed a significant increase in c-Fos mRNA
261 accumulation following DFP poisoning (Figure 2B, $p < 0.001$), suggesting increased neuronal
262 excitation. We then sought to visualize neuronal activity in live brains of larvae exposed to DFP
263 using calcium imaging. Indeed, transient calcium uptakes in neurons, as revealed by GCaMP5G
264 fluorescent protein, fully correlates neuronal excitation in zebrafish epilepsy models, allowing to
265 visualize seizures in vivo at the level of a whole brain[11,35]. Five dpf larvae from the transgenic line
266 Tg[Huc:GCaMP5G] were treated with DFP and neuronal activity was recorded during the 6 h of
267 incubation time using time-lapse confocal microscopy (Figure 2E, and supplementary video 2). As
268 early as 20 min following DFP addition, some intense transient calcium uptake events were
269 detected; their number and intensity progressively increased over the next 2 hours (Figure 2F, G).
270 Then, 2 - 3 hours following DFP addition, all DFP-treated larvae (n = 5) displayed massive, brief
271 and synchronous calcium uptake events in both neuropils of the optic tectum neurons, strongly
272 reminiscent of those seen during generalized seizures in zebrafish epilepsy models (Figure 2C2).

273 To confirm that the increase in neuronal calcium uptakes observed in DFP-exposed larvae
274 did correspond to actual neuronal hyperexcitation, we ascertained whether administration of

275 diazepam, the main drug administered to epileptic patients to relieve seizures[36], alleviated calcium
276 uptake activity. Larvae were first exposed to DFP (15 μM) for 5 h, and their neuronal calcium
277 activity was recorded for 30 minutes; diazepam (40 μM) was then added and their neuronal calcium
278 activity was recorded for an additional 60 min. Interestingly, exposure to diazepam significantly
279 decreased neuronal excitation induced by DFP (Figure 2H, I). All these data confirm that DFP
280 exposure caused an intense neuronal hyperexcitation.

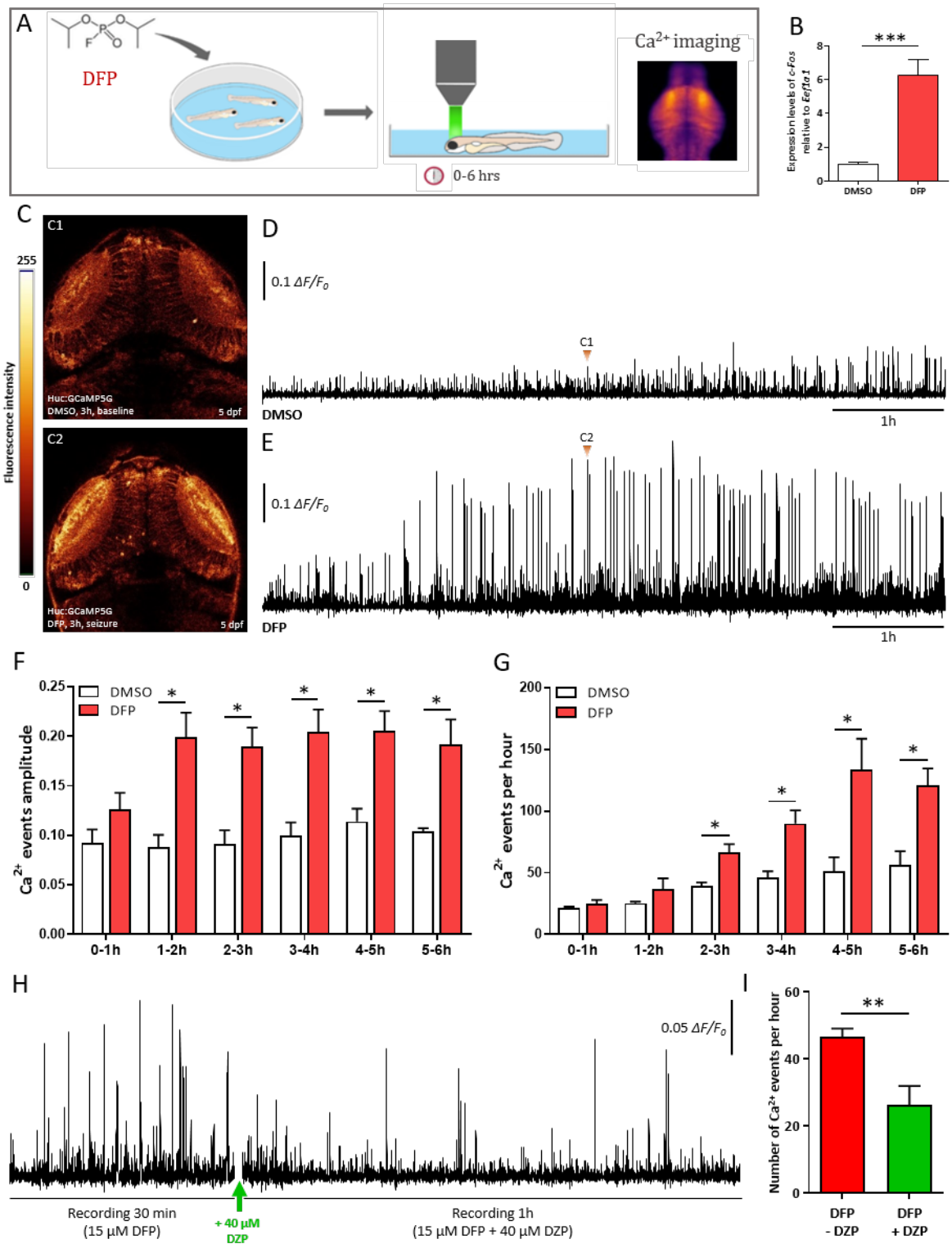

281

282 **Figure 2.** DFP exposure caused increased neuron excitation. **A**: In the experimental set-up, 5 dpf

283 Tg[Huc:GCaMP5G] larvae were exposed to either 15 μM DFP or vehicle (DMSO), and transient

284 calcium uptakes were then recorded in brain neurons over 6 h using calcium imaging. **B**: qRT-PCR
285 demonstrated markedly increased expression of the *C-Fos* gene in larvae exposed to 15 μM DFP
286 (n = 19) when compared to that in control larvae (DMSO) (n = 19) (Student unpaired t-test: ***, p
287 < 0.001). **C**, Snapshot views of calcium imaging of 5 dpf Tg[Huc:GCaMP5G] larvae brain showing
288 baseline calcium activity (C1 in Figure 2D) and seizure-like hyperactivity (C2 in Figure 2E) seen
289 3 h after 15 μM DFP exposure. **D**: Transient calcium uptakes in 5 dpf Tg[Huc:GCaMP5G] larvae
290 treated with vehicle (DMSO) (n = 5). **E**: Transient calcium uptakes in 5 dpf Tg[Huc:GCaMP5G]
291 larvae exposed to 15 μM DFP (n = 5). **F**: Amplitude of calcium uptake events in 5 dpf
292 Tg[Huc:GCaMP5G] larvae at different time points during exposure to either 15 μM DFP (n = 5)
293 or vehicle (DMSO) (n = 5) (Student unpaired t-test: *, p < 0.05). **G**: Number of calcium uptake
294 events showing $\Delta F/F_0 > 0.04$ in 5 dpf Tg[Huc:GCaMP5G] larvae at different time points during
295 exposure to either 15 μM DFP (n = 5) or vehicle (DMSO) (n = 5) (Student unpaired t-test: *, p <
296 0.05). **H**: Pattern of transient calcium uptake events in 5 dpf Tg[Huc:GCaMP5G] larvae exposed
297 to 15 μM DFP for 5 h and then to 15 μM DFP + 40 μM diazepam (DZP) for one more hour. **I**:
298 Number of calcium uptake events showing $\Delta F/F_0 > 0.04$ in 5 dpf Tg[Huc:GCaMP5G] larvae
299 exposed to either 15 μM DFP or 15 μM DFP + 40 μM diazepam (DZP) (Student unpaired t-test: p
300 = 0.009).

301 Exposure to highly toxic OP compounds (soman, sarin, VX) has been shown to cause
302 elevated neuronal loss in both humans and animal models[24,37–40]. We thus examined whether the
303 larvae exposed to DFP showed an increase in neuronal death. Using acridine orange (AO), a vital
304 marker that labels dying cells, we first observed in living larvae a marked increase in the number
305 of cells showing AO staining in DFP-exposed larvae compared to controls (Figure 3C, D, E). Anti-

306 activated-caspase-3 immunolabeling confirmed that DFP exposure promotes neuronal apoptosis

307 (Figure 3F, G, H).

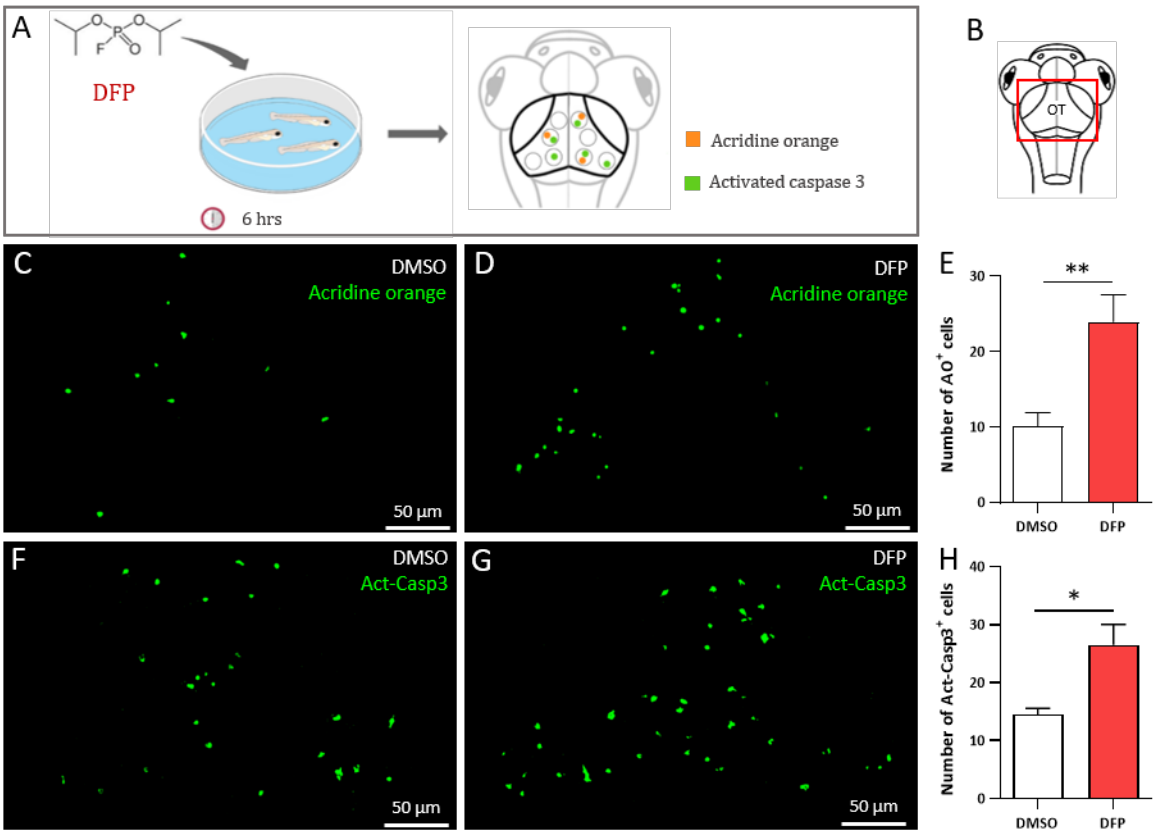

308

309 **Figure 3.** DFP exposure promoted increased neuron apoptosis. **A**: In the experimental set-up, 5 dpf

310 larvae were exposed to either 15 μM DFP or vehicle (DMSO) for 6 h, prior to acridine orange

311 staining or anti-activated caspase-3 immunolabeling. **B**: Scheme of 5 dpf larvae head with the red

312 box showing the region of interest in the brain uncovering the optic tectum (OT). **C** and **D**: Acridine

313 orange labeling of dead neuronal cells in 5 dpf larvae exposed for 6 h to either vehicle (DMSO)

314 (C) or 15 μM DFP (D). Scale bar: 50 μm. **E**: Number of acridine orange-positive cells in 5 dpf

315 larvae exposed for 6 h to either vehicle (DMSO) (n = 8) or 15 μM DFP (n = 10) (Student unpaired

316 t-test: p = 0.002). **F** and **G**: Anti-activated caspase-3 (Act-Casp3) immunolabeling of dying

317 neuronal cells in 5 dpf larvae exposed for 6 h to either vehicle (DMSO) (F) or 15 μM DFP (G).

318 Scale bar: 50 μm. **H**: Number of activated-caspase-3 positive cells in 5 dpf larvae exposed for 6 h
319 to either vehicle (DMSO) (n = 7) or 15 μM DFP (n = 8) (Student unpaired t-test with Welch's
320 correction: p = 0.01).

321 **3.5 Increased NR2B-NMDA receptor expression and decreased GAD65/67 and gephyrin**
322 **protein accumulation in DFP exposed larvae**

323 It has been shown that following OP exposure, AChE inhibition causes an acute stimulation
324 of cholinergic receptors, inducing increased neuronal glutamatergic response, and excessive
325 NMDA receptor activation[41–43]. To examine whether accumulation of the NR2B-NMDA receptor
326 sub-unit, a major excitatory glutamate receptor, was affected following DFP exposure, brain
327 sections of larvae exposed to DFP and control siblings were analyzed by immunocytochemistry
328 using an anti-NR2B-NMDA receptor antibody (Figure 4A, excitatory synapse). Interestingly,
329 results showed a clear increase in NR2B-NMDA accumulation in the brains of DFP-exposed
330 larvae, compared to untreated controls (Figure 4C, Supplementary video 3 and 4). The increased
331 NR2B-NMDA accumulation induced by DFP poisoning was confirmed by quantification of
332 NR2B-NMDA staining using Imaris software (Bitplane Inc., Version 9.1.2) (Figure 4G). To further
333 characterize neuronal networks in DFP-treated larvae, we analyzed the accumulation of glutamate
334 decarboxylase (GAD65/67), an enzyme involved in GABA synthesis in presynaptic inhibitory
335 synapses, and gephyrin, a protein that anchors postsynaptic GABA receptors to the cytoskeleton,
336 using anti-GAD65/67 and anti-gephyrin antibodies, respectively (Figure 4A, inhibitory synapse).
337 Interestingly, following DFP exposure, we observed a significant decrease in the accumulation of
338 both GAD65/67 (Figure 4D) and gephyrin (Figure 4F). Labeling quantification using Imaris

339 software (Bitplane Inc., Version 9.1.2) confirmed the decreased accumulation of both GAD65/67

340 (Figure 4H) and gephyrin in DFP-treated larvae (Figure 4I).

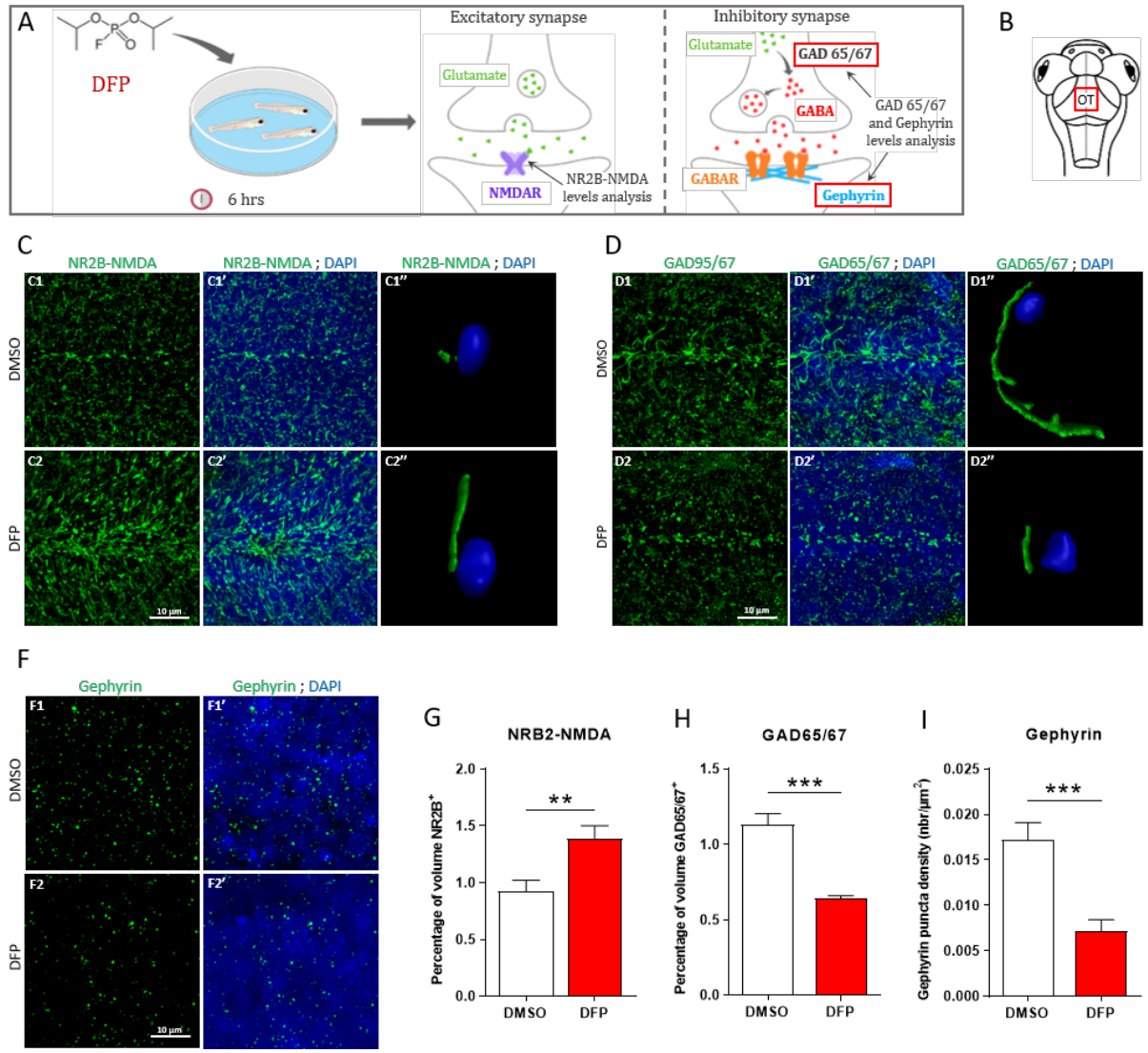

341

342 **Figure 4.** DFP exposure provoked increased NR2B-NMDA receptor accumulation. **A**: As

343 experimental set-up, 5 dpf larvae were exposed to either 15 μM DFP or vehicle (DMSO) for 6

344 hours, prior to NR2B-NMDA immunolabelling of glutamatergic/excitatory synapses. **B**: Scheme

345 of 5 dpf larvae head with the red box showing the region of interest in the brain uncovering the

346 optic tectum (OT). **C**: Anti-NR2B-NMDA receptor immunolabelling of glutamatergic synapses

347 (C1 to C2') and DAPI staining (C1', C2') in 5 dpf larvae exposed for 6 hours to either vehicle
348 (DMSO) (C1, C1') or 15 μM DFP (C2, C2'). Scale bar: 10 μm. 3D image reconstruction of NR2B-
349 NMDA labeled neuron branch details in 5 dpf larvae exposed for 6 hours to either vehicle (DMSO)
350 (C1'') or 15 μM DFP (C2''). **D**: Anti-GAD 65/67 immunolabeling of GABAergic presynapses (D1
351 to D2') and DAPI staining (D1', D2') in 5 dpf larvae exposed for 6 h to either vehicle (DMSO) (D1,
352 D1') or 15 μM DFP (D2, D2'). Scale bar: 10 μm. D, 3D image reconstruction of GAD 65/67 labeled
353 neuron branch details in 5 dpf larvae exposed for 6 h to either vehicle (DMSO) (D1'') or 15 μM
354 DFP (D2''). **F:** Anti-gephyrin immunolabeling of GABAergic presynapses (F1 to F2') and DAPI
355 staining (F1', F2') in 5 dpf larvae exposed for 6 h to either vehicle (DMSO) (F1, F1') or 15 μM DFP
356 (F2, F2'). Scale bar: 10 μm. **G**: Quantification of the volume of NR2B-NMDA labeled branch
357 material in 5 dpf larvae treated for 6 hours with either vehicle (DMSO) (n = 13) or 15 μM DFP (n
358 = 13) (Student unpaired t-test: $p = 0.004$). **H**: Quantification of the volume of GAD 65/67 labeled
359 branch material in 5 dpf larvae treated for 6 h with either vehicle (DMSO) (n = 14) or 15 μM DFP
360 (n = 14) (Student unpaired t-test with Welch's correction: ***, $p < 0.001$). **I**: Quantification of the
361 density of gephyrin puncta in 5 dpf larvae treated for 6 h with either vehicle (DMSO) (n = 20) or
362 15 μM DFP (n = 20) (Mann-Whitney: ***, $p < 0.001$).

363 **4. DISCUSSION**

364 Because of their use for agricultural purposes worldwide, acute poisoning by OP
365 compounds is a major public health problem, with several millions of intoxications reported each
366 year[44,45]. In this work, we took advantage of the possibilities offered by zebrafish larvae to develop
367 an animal model of OP poisoning and study the consequences of OP exposure on neuronal network
368 activity. Interestingly, as described in mammalian models of OP poisoning[46,47], zebrafish larvae

369 exposed to DFP displayed marked AChE inhibition, the hallmark of OP intoxication, validating
370 this small fish as a good model for investigating the consequences of OP poisoning. One of the
371 most devastating features of OP intoxication in both humans and rodents is full, sometimes fatal,
372 respiratory failure[28]. It is important to note that in epileptic OP intoxication models that use
373 mammals, the induced respiratory failure must be prevented by the simultaneous addition of
374 cholinergic inhibitors (atropine) and AChE reactivators (oximes) to avoid premature death[29]. By
375 contrast, although we observed that DFP-treated larvae showed significantly decreased oxygen
376 consumption, there was no need to protect larvae with cholinergic inhibitors. Thus, DFP-exposed
377 zebrafish larvae appeared as a powerful and simple model to test the effects of anti-convulsive
378 agents in absence of either muscarinic antagonists or cholinesterase reactivators.

379 It has been demonstrated that acute OP exposure causes epileptic-like seizures, which, if
380 not treated, can eventually lead to life-threatening status epilepticus[47]. We therefore investigated
381 neuronal excitation in larvae exposed to DFP. We first found that larvae exposed to DFP showed
382 increased expression of c-Fos, a marker of neuronal activity, which is overexpressed after
383 seizures[48–50]. We next recorded neuronal calcium uptakes in living larvae exposed to DFP, a
384 technology that enables visualization of epileptic seizures[11,35]. In DFP-exposed larvae, as early as
385 20 minutes following OP addition, we observed neurons showing massive calcium uptake events
386 that were never seen in control siblings, and which number increased over the next 2 h. Moreover,
387 the OP-induced neuronal activity was potently alleviated by diazepam treatment, confirming that
388 larvae exposed to DFP show neuronal hyperexcitation reflecting epileptiform seizures. In humans,
389 if victims are not treated within the first 30 minutes, seizures caused by OP intoxication can end in
390 status epilepticus, a major life-threatening neurologic disorder[6,51], also leading to long term brain
391 damages[52,53]. This 30-minute long status epilepticus window frame also appears to be a critical

392 period during which long-term brain lesions are generated[51]. In the Tokyo subway attack,
393 approximately 3% of OP-poisoned victims suffered convulsions[54]. Interestingly, 2 - 3 h after DFP
394 exposure, we observed that all the DFP-exposed larvae showed massive synchronous calcium
395 uptake events, strongly reminiscent of generalized seizures seen in zebrafish epilepsy models[11,35],
396 suggesting that these larvae displayed a status epilepticus-like phenotype.

397 Together with AChE inhibition and neuronal seizures, massive neuronal death is another
398 hallmark of OP poisoning[20], also observed in the DFP-exposed zebrafish larvae. At the cellular
399 level, it has long been known that hyperactivity of cholinergic receptors induces a massive release
400 of glutamate, leading to over-activation of glutamatergic receptors and neuronal
401 hyperexcitability[41–43]. Specifically, it has been shown that acute OP intoxication induces the
402 activation of NMDA receptors[55]. Moreover, in a mammalian model of OP poisoning, activation of
403 NMDA receptors plays essential roles in seizure activity and apoptosis[52,56]. In the brain of zebrafish
404 larvae exposed to DFP, we observed a decreased accumulation of both gephyrin and GAD65/67,
405 two proteins specifically accumulated in inhibitory synapses, while NR2B-NMDA receptor was
406 significantly overexpressed. This suggests that following acute DFP poisoning, neuronal
407 hyperexcitation results from a shift in the synaptic balance of brain neurons toward excitatory
408 states.

409 We report here a vertebrate model of OP poisoning that displays phenotypes and symptoms
410 of acute toxicity, faithfully recapitulating those described in humans, i.e. AChE inhibition,
411 respiratory deficit, neuronal apoptosis and epileptiform seizures. The zebrafish is thus a model of
412 choice for large-scale screening of entities that could restore CNS functions after OP poisoning and
413 mitigate the long-term neurological sequelae of acute OP poisoning in humans.

414 **ACKNOWLEDGMENTS**

415 We thank Christiane Romain (Inserm UMR 1141) and Olivier Bar (Inserm UMR 1141).

416 **DISCLOSURE**

417 The authors declare that the research was conducted in the absence of any commercial or financial

418 relationships that could be construed as a potential conflict of interest.

419 **SUPPLEMENTARY MATERIAL**

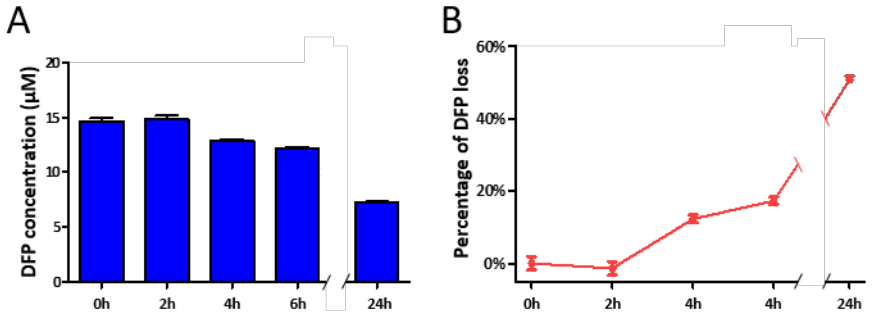

420
421 **Figure S1.** Monitoring the stability of DFP diluted in FW. A: Residual concentrations of DFP

422 measured at different time points following dilution to 15 μM in FW. B: Percentage of DFP loss

423 over time showing a 2% loss per hour, approximately.

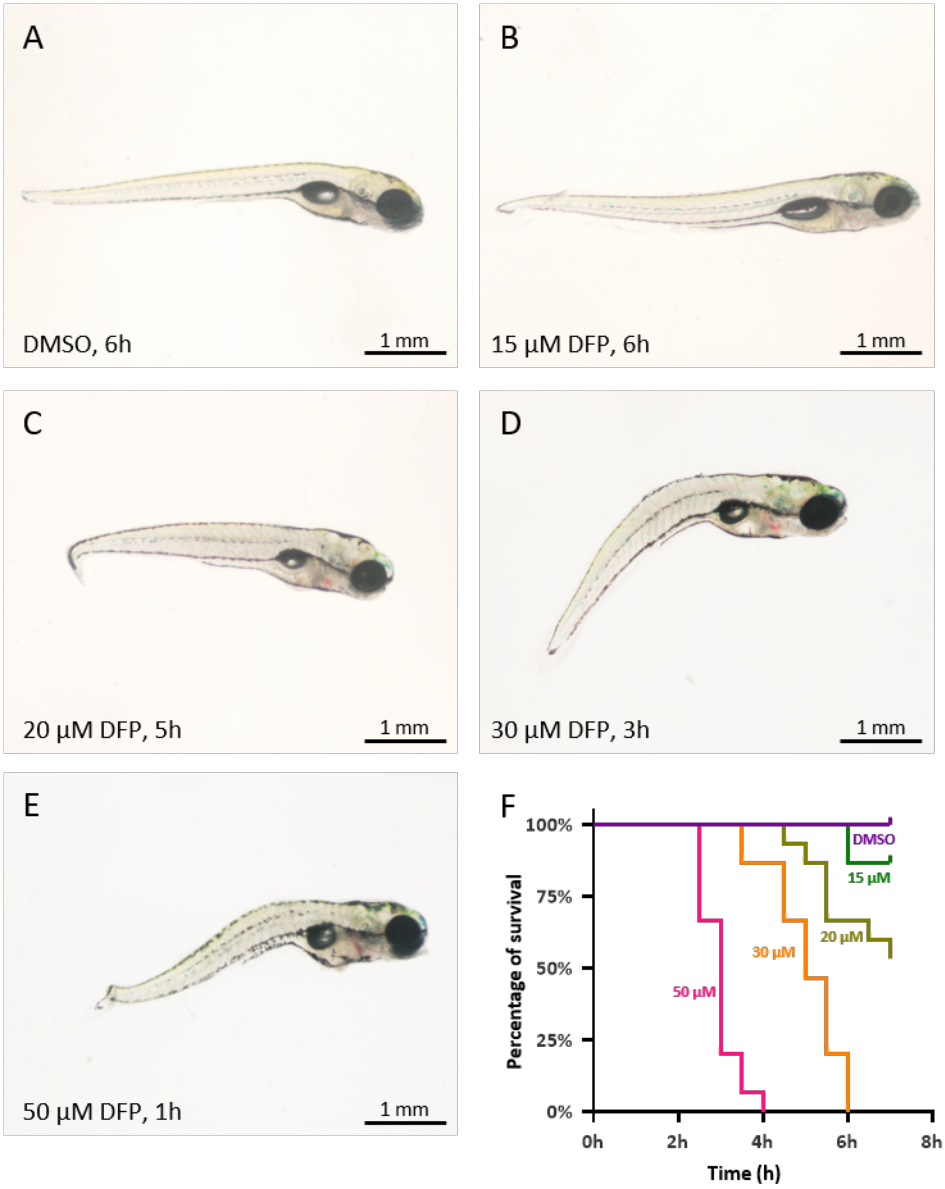

Figure S2. DFP exposure caused phenotypic defects and larval lethality. A-E: Phenotypes of 5 dpf larvae exposed to either vehicle (DMSO) for 6 h (A), or 15 μM DFP for 6 h (B), or 20 μM DFP for 5 h (C), or 30 μM DFP for 3 h (D), or 50 μM for 1 h (E). Scale bar: 1 mm. F: Survival curve of 5 dpf larvae exposed to either vehicle (DMSO) or 15, 20, 30 or 50 μM DFP.

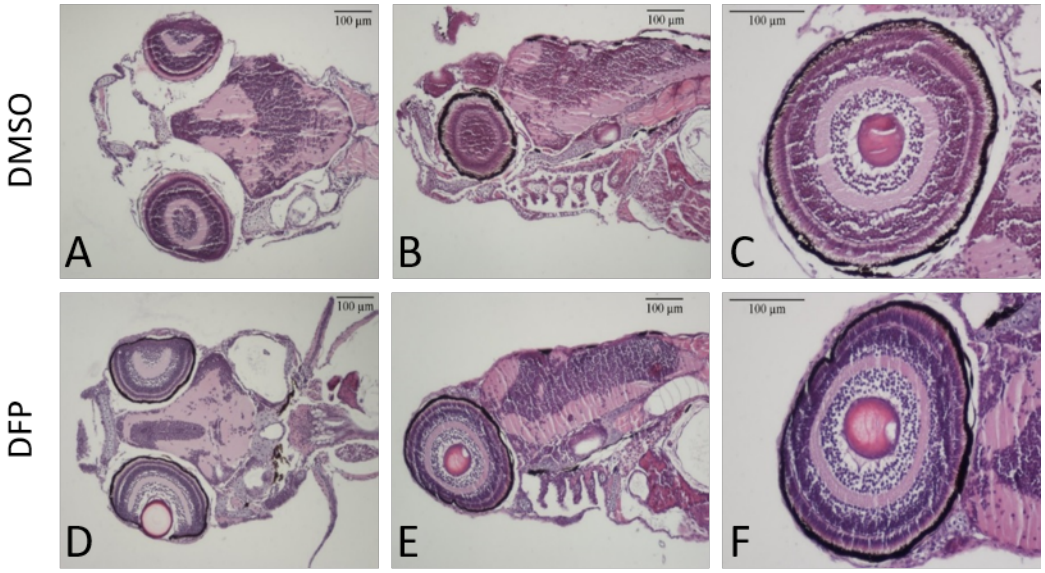

429
430 **Figure S3.** Zebrafish larvae exposed for 6 h to 15 μM DFP do not show visible phenotypic defects.
431 A-F Horizontal (A, D) and sagittal (B, C, E, F) tissue sections of 5 dpf larvae (A, B, D, E) and
432 corresponding eyes (C, F), following exposure for 6 h to either vehicle (DMSO) (A, B, C) or 15
433 μM DFP (D, E, F).

434 **Supplementary Video 1.** 3 minute-long representative recording of calcium activity imaging in
435 optic tectum neurons of 5 dpf larvae following 3 h exposure to vehicle (DMSO). Movie played at
436 25 fps.

437 **Supplementary Video 2.** 3 minute-long representative recording of calcium activity imaging in
438 optic tectum neurons of 5 dpf larvae following 3 h exposure to 15 μM DFP. Movie played at 25
439 fps.

440 **Supplementary Video 3.** 3D reconstruction of the image depicted in Figure 4C1', showing the
441 optic tectum from a 5 dpf larva exposed for 6 hto vehicle (DMSO) and labeled with an anti-NR2B-
442 NMDA antibody (green) and counterstained with DAPI (blue). 3D images were generated using
443 Imaris software (Bitplane Inc., Version 9.1.2).

444 **Supplementary Video 4.** 3D reconstruction of the image depicted in Figure 4C2', showing the
445 optic tectum from a 5 dpf larva exposed for 6 h to 15 μM DFP and labeled with an anti-NR2B-
446 NMDA antibody (green) and counterstained with DAPI (blue). 3D images were generated using
447 Imaris software (Bitplane Inc., Version 9.1.2).

448 **Supplementary Video 5.** 3D reconstruction of the image depicted in Figure 5C1', showing the
449 optic tectum from a 5 dpf larva exposed for 6 h to vehicle (DMSO) and labeled with an anti-GAD
450 65/67 antibody (green) and counterstained with DAPI (blue). 3D images were generated using
451 Imaris software (Bitplane Inc., Version 9.1.2).

452 **Supplementary Video 6.** 3D reconstruction of the image depicted in Figure 5C2', showing the
453 optic tectum from a 5 dpf larva exposed for 6 h to 15 μM DFP and labeled with an anti-GAD 65/67
454 antibody (green) and counterstained with DAPI (blue). 3D images were generated using Imaris
455 software (Bitplane Inc., Version 9.1.2).

456 **Funding**: This work was supported by Institut National de la Santé et la Recherche Médicale
457 (INSERM), the Centre National de la Recherche Scientifique (CNRS), the French National
458 Research Agency (ANR-16-CE18-0010), and Fondation NRJ (Institut de France), and the Agence
459 de l'Innovation de Défense. Funding sources had no involvement in study design, collection,
460 analysis or interpretation of data, or decision to publish.

461 **Author Contributions**: A.B., performed the experiments, the analysis, and designed the figures.
462 N.S.Y. supervised the project and wrote the manuscript. J.S., performed the respiratory
463 experiments, R.H.A., R.L, M.P., A.I., D.S., and N.T. helped carry out the experiments .N.D. helped
464 supervise the project. C.Y. G.D.B., F.N., N.D, contributed to the final manuscript.

465 **REFERENCES:**

466 1. Mew EJ, Padmanathan P, Konradsen F, et al. The global burden of fatal self-poisoning with
467 pesticides 2006-15: Systematic review. *J Affect Disord*. 2017;219(May):93-104.
468 doi:10.1016/j.jad.2017.05.002

469 2. Konickx LA, Worek F, Jayamanne S, Thiermann H, Buckley NA, Eddleston M. Reactivation
470 of Plasma Butyrylcholinesterase by Pralidoxime Chloride in Patients Poisoned by WHO
471 Class II Toxicity Organophosphorus Insecticides. 2013. doi:10.1093/toxsci/kft217

472 3. Pereira EFR, Aracava Y, Detolla LJ, et al. Animal Models That Best Reproduce the Clinical
473 Manifestations of Human Intoxication with Organophosphorus Compounds. *J Pharmacol*
474 *Exp Ther J Pharmacol Exp Ther*. 2014;350:313-321. doi:10.1124/jpet.114.214932

475 4. Jett DA. Neurological aspects of chemical terrorism. *Ann Neurol*. 2007;61(1):9-13.
476 doi:10.1002/ana.21072

477 5. Lotti M. Clinical Toxicology of Anticholinesterase Agents in Humans. In: *Hayes' Handbook*
478 *of Pesticide Toxicology*. Elsevier Inc.; 2010:1543-1589. doi:10.1016/B978-0-12-374367-
479 1.00072-0

480 6. Todorovic MS, Cowan ML, Balint CA, Sun C, Kapur J. Characterization of status epilepticus
481 induced by two organophosphates in rats. *Epilepsy Res*. 2012;101(3):268-276.
482 doi:10.1016/j.eplepsyres.2012.04.014

483 7. Chen Y. Organophosphate-induced brain damage: mechanisms, neuropsychiatric and
484 neurological consequences, and potential therapeutic strategies. *Neurotoxicology*.
485 2012;33(3):391-400. doi:10.1016/j.neuro.2012.03.011

486 8. Collombet J-M. Nerve agent intoxication: Recent neuropathophysiological findings and
487 subsequent impact on medical management prospects. 2011.
488 doi:10.1016/j.taap.2011.07.003

489 9. Yanicostas C, Ernest S, Dayraud C, Petit C, Soussi-Yanicostas N. Essential requirement for
490 zebrafish anosmin-1a in the migration of the posterior lateral line primordium. *Dev Biol*.
491 2008;320(2):469-479. doi:10.1016/j.ydbio.2008.06.008

492 10. Martin E, Yanicostas C, Rastetter A, et al. Spatacsin and spastizin act in the same pathway
493 required for proper spinal motor neuron axon outgrowth in zebrafish. *Neurobiol Dis*.
494 2012;48(3):299-308. doi:10.1016/j.nbd.2012.07.003

495 11. Brenet A, Hassan-Abdi R, Somkhit J, Yanicostas C, Soussi-Yanicostas N. Defective
496 Excitatory/Inhibitory Synaptic Balance and Increased Neuron Apoptosis in a Zebrafish

497 Model of Dravet Syndrome. *Cells*. 2019;8(10):1199. doi:10.3390/cells8101199

498 12. Ghoumid J, Drevillon L, Alavi-Naini SM, et al. ZEB2 zinc-finger missense mutations lead to
499 hypomorphic alleles and a mild Mowat-Wilson syndrome. *Hum Mol Genet*.
500 2013;22(13):2652-2661. doi:10.1093/hmg/ddt114

501 13. Yanicostas C, Barbieri E, Hibi M, Brice A, Stevanin G, Soussi-Yanicostas N. Requirement for
502 Zebrafish Ataxin-7 in Differentiation of Photoreceptors and Cerebellar Neurons. *PLoS One*.
503 2012;7(11). doi:10.1371/journal.pone.0050705

504 14. MacRae CA, Peterson RT. Zebrafish as tools for drug discovery. *Nat Rev | DRUG Discov*.
505 2015;14:721-731. doi:10.1038/nrd4627

506 15. Lessman CA. The developing zebrafish (Danio rerio): A vertebrate model for high-
507 throughput screening of chemical libraries. *Birth Defects Res Part C - Embryo Today Rev*.
508 2011;93(3):268-280. doi:10.1002/bdrc.20212

509 16. Delvecchio C, Tiefenbach J, Krause HM. The Zebrafish: A powerful platform for in vivo, HTS
510 drug discovery. *Assay Drug Dev Technol*. 2011;9(4):354-361. doi:10.1089/adt.2010.0346

511 17. Rinkwitz S, Mourrain P, Becker TS. Zebrafish: An integrative system for neurogenomics and
512 neurosciences. *Prog Neurobiol*. 2011;93(2):231-243. doi:10.1016/j.pneurobio.2010.11.003

513 18. Ito H, Yamamoto N. Non-laminar cerebral cortex in teleost fishes? *Biol Lett*. 2009;5(1):117-
514 121. doi:10.1098/rsbl.2008.0397

515 19. Wullimann MF. Secondary neurogenesis and telencephalic organization in zebrafish and
516 mice: a brief review. *Integr Zool*. 2009;4(1):123-133. doi:10.1111/j.1749-
517 4877.2008.00140.x

518 20. Flannery BM, Bruun DA, Rowland DJ, et al. Persistent neuroinflammation and cognitive
519 impairment in a rat model of acute diisopropylfluorophosphate intoxication. *J*
520 *Neuroinflammation*. 2016;13(1):1-16. doi:10.1186/s12974-016-0744-y

521 21. Li Y, Lein PJ, Liu C, et al. Spatiotemporal pattern of neuronal injury induced by DFP in rats:
522 A model for delayed neuronal cell death following acute OP intoxication. *Toxicol Appl*
523 *Pharmacol*. 2011;253(3):261-269. doi:10.1016/j.taap.2011.03.026

524 22. Auta J, Costa E, Davis J, Guidotti A. Imidazenil: a potent and safe protective agent against
525 diisopropyl fluorophosphate toxicity. *Neuropharmacology*. 2004;46(3):397-403.
526 doi:10.1016/j.neuropharm.2003.09.010

527 23. Deshpande LS, Carter DS, Blair RE, DeLorenzo RJ. Development of a Prolonged Calcium
528 Plateau in Hippocampal Neurons in Rats Surviving Status Epilepticus Induced by the

529 Organophosphate Diisopropylfluorophosphate. *Toxicol Sci*. 2010;116(2):623-631.
530 doi:10.1093/toxsci/kfq157

531 24. Kim YB, Hur GH, Shin S, Sok DE, Kang JK, Lee YS. Organophosphate-induced brain injuries:
532 delayed apoptosis mediated by nitric oxide. *Environ Toxicol Pharmacol*. 1999;7(2):147-152.
533 http://www.ncbi.nlm.nih.gov/pubmed/21781920. Accessed September 2, 2019.

534 25. Wright LKM, Liu J, Nallapaneni A, Pope CN. Behavioral sequelae following acute
535 diisopropylfluorophosphate intoxication in rats: comparative effects of atropine and
536 cannabinomimetics. *Neurotoxicol Teratol*. 2010;32(3):329-335.
537 doi:10.1016/j.ntt.2009.12.006

538 26. McDonough JH, Shih TM. Neuropharmacological mechanisms of nerve agent-induced
539 seizure and neuropathology. *Neurosci Biobehav Rev*. 1997;21(5):559-579.
540 http://www.ncbi.nlm.nih.gov/pubmed/9353792. Accessed September 2, 2019.

541 27. Yamasue H, Abe O, Kasai K, et al. Human brain structural change related to acute single
542 exposure to sarin. *Ann Neurol*. 2007;61(1):37-46. doi:10.1002/ana.21024

543 28. Giyanwani PR, Zubair U, Salam O, Zubair Z. Respiratory Failure Following Organophosphate
544 Poisoning: A Literature Review. 2017. doi:10.7759/cureus.1651

545 29. Carey JL, Dunn C, Gaspari RJ. Central respiratory failure during acute organophosphate
546 poisoning. *Respir Physiol Neurobiol*. 2013;189(2):403-410. doi:10.1016/j.resp.2013.07.022

547 30. Szyndler J, Maciejak P, Turzyńska D, et al. Mapping of c-Fos expression in the rat brain
548 during the evolution of pentylenetetrazol-kindled seizures. *Epilepsy Behav*.
549 2009;16(2):216-224. doi:10.1016/j.yebeh.2009.07.030

550 31. Iryo Y, Matsuoka M, Igisu H. Suppression of pentylenetetrazol-induced seizures and c-fos
551 expression in mouse brain by L-carnitine. *J Occup Health*. 2000;42(3):119-123.
552 doi:10.1539/joh.42.119

553 32. Morgan JI, Cohen DR, Hempstead JL, Curran T. Mapping patterns of c-fos expression in the
554 central nervous system after seizure. *Science (80-)*. 1987;237(4811):192-197.
555 doi:10.1126/science.3037702

556 33. Clark M, Post RM, Weiss SR, Cain CJ, Nakajima T. Regional expression of c-fos mRNA in rat
557 brain during the evolution of amygdala kindled seizures. *Brain Res Mol Brain Res*.
558 1991;11(1):55-64. doi:10.1016/0169-328x(91)90021-o

559 34. Burazin TCD, Gundlach AL. Rapid and transient increases in cellular immediate early gene
560 and neuropeptide mRNAs in cortical and limbic areas after amygdaloid kindling seizures in
561 the rat. In: *Epilepsy Research*. Vol 26. ; 1996:281-293. doi:10.1016/S0920-1211(96)00060-

562 5

563 35. Liu J, Baraban SC. Network Properties Revealed during Multi-Scale Calcium Imaging of
564 Seizure Activity in Zebrafish. *eNeuro*. 2019;6(1):ENEURO.0041-19.2019.
565 doi:10.1523/ENEURO.0041-19.2019

566 36. Verrotti A, Milioni M, Zaccara G. Safety and efficacy of diazepam autoinjector for the
567 management of epilepsy. *Expert Rev Neurother*. 2014;15(2):127-133.
568 doi:10.1586/14737175.2015.1003043

569 37. Petras JM. NEUROLOGY AND NEUROPATHOLOGY OF SOMAN-INDUCED BRAIN INJURY: AN
570 OVERVIEW. *J Exp Anal Behav*. 1994;61(2):319-329. doi:10.1901/jeab.1994.61-319

571 38. Shih T-M, Duniho SM, Mcdonough JH. Control of nerve agent-induced seizures is critical for
572 neuroprotection and survival. 2003. doi:10.1016/S0041-008X(03)00019-X

573 39. Kaur P, Radotra B, Minz RW, Gill KD. Impaired mitochondrial energy metabolism and
574 neuronal apoptotic cell death after chronic dichlorvos (OP) exposure in rat brain. 2007.
575 doi:10.1016/j.neuro.2007.08.001

576 40. Gunay N, Kose B, Demiryurek S, Ceylan NO, Sari I, Demiryurek AT. Protective effects of Y-
577 27632 on acute dichlorvos poisoning in rats. *Am J Emerg Med*. 2010;28(3):268-274.
578 doi:10.1016/j.ajem.2008.11.020

579 41. Lallement G, Carpentier P, Pernot-Marino I, Baubichon D, Collet A, Blanchet G. Involvement
580 of the different rat hippocampal glutamatergic receptors in development of seizures
581 induced by soman: an autoradiographic study. *Neurotoxicology*. 1991;12(4):655-664.
582 http://www.ncbi.nlm.nih.gov/pubmed/1665552. Accessed November 20, 2019.

583 42. Lallement G, Carpentier P, Collet A, et al. Involvement of glutamatergic system of amygdala
584 in generalized seizures induced by soman: comparison with the hippocampus. *C R Acad Sci*
585 *III*. 1991;313(9):421-426. http://www.ncbi.nlm.nih.gov/pubmed/1836748. Accessed
586 November 20, 2019.

587 43. Lallement G, Carpentier P, Collet A, Pernot-Marino I, Baubichon D, Blanchet G. Effects of
588 soman-induced seizures on different extracellular amino acid levels and on glutamate
589 uptake in rat hippocampus. *Brain Res*. 1991;563(1-2):234-240. doi:10.1016/0006-
590 8993(91)91539-D

591 44. Dawson AH, Eddleston M, Senarathna L, et al. Acute human lethal toxicity of agricultural
592 pesticides: A prospective cohort study. *PLoS Med*. 2010;7(10).
593 doi:10.1371/journal.pmed.1000357

594 45. Bertolote JM, Fleischmann A, Eddleston M, Gunnell D. Deaths from pesticide poisoning: a

595 global response. *Br J Psychiatry*. 2006;189(3):201-203. doi:10.1192/bjp.bp.105.020834

596 46. McCarren HS, McDonough JH. Anticonvulsant discovery through animal models of status
597 epilepticus induced by organophosphorus nerve agents and pesticides. *Ann N Y Acad Sci*.
598 2016;1374(1):144-150. doi:10.1111/nyas.13092

599 47. Todorovic M, Cowan M, Balint C, Sun C, Kapur J. Characterization of status epilepticus
600 induced by two organophosphates in rats. 2012. doi:10.1016/j.eplepsyres.2012.04.014

601 48. Dragunow M, Robertson HA. Kindling stimulation induces c-fos protein(s) in granule cells
602 of the rat dentate gyrus. *Nature*. 1987;329(6138):441-442. doi:10.1038/329441a0

603 49. Le Gal G, Salle L. *Long-Lasting and Sequential Increase of c-Fos Oncoprotein Expression in*
604 *Kainic Acid-Induced Status Epilepticus*. Vol 88.; 1988.

605 50. Simler S, Hirsch E, Danober L, Motte J, Vergnes M, Marescaux C. C-fos expression after
606 single and kindled audiogenic seizures in Wistar rats. *Neurosci Lett*. 1994;175(1-2):58-62.
607 doi:10.1016/0304-3940(94)91077-4

608 51. Trinka E, Cock H, Hesdorffer D, et al. A definition and classification of status epilepticus -
609 Report of the ILAE Task Force on Classification of Status Epilepticus. *Epilepsia*.
610 2015;56(10):1515-1523. doi:10.1111/epi.13121

611 52. Shih TM, McDonough JH. Neurochemical mechanisms in soman-induced seizures. *J Appl*
612 *Toxicol*. 1997;17(4):255-264. doi:10.1002/(SICI)1099-1263(199707)17:4<255::AID-
613 JAT441>3.0.CO;2-D

614 53. Tryphonas L, Clement JG. Histomorphogenesis of soman-induced
615 encephalocardiomyopathy in Sprague- Dawley rats. *Toxicol Pathol*. 1995;23(3):393-409.
616 doi:10.1177/019262339502300316

617 54. Okumura T, Takasu N, Ishimatsu S, et al. Report on 640 victims of the Tokyo subway sarin
618 attack. *Ann Emerg Med*. 1996;28(2):129-135. doi:10.1016/S0196-0644(96)70052-5

619 55. Kaur S, Singh S, Chahal KS, Prakash A. Potential pharmacological strategies for the improved
620 treatment of organophosphate-induced neurotoxicity. *Can J Physiol Pharmacol*.
621 2014;92(11):893-911. doi:10.1139/cjpp-2014-0113

622 56. Solberg Y, Belkin M. The role of excitotoxicity in organophosphorous nerve agents central
623 poisoning. *Trends Pharmacol Sci*. 1997;18(6):183-185. doi:10.1016/S0165-6147(97)89540-
624 5

625